ACADEMIC PRESS

Available online at www.sciencedirect.com

SCIENCE DIRECT®

Journal of Sound and Vibration 263 (2003) 357–376

JOURNAL OF SOUND AND VIBRATION

www.elsevier.com/locate/jsvi

Active isolation of a flexible structure from base vibration

X. Huang*, S.J. Elliott, M.J. Brennan

Signal Processing and Control Group, Institute of Sound and Vibration Research, University of Southampton, Highfield, Southampton SO17 1BJ, UK

Received 20 December 2001; accepted 23 May 2002

Abstract

This paper presents a theoretical and experimental investigation into an active vibration isolation system. Electromagnetic actuators are installed in parallel with each of four passive mounts, which are placed between a flexible equipment structure and a base structure which is either flexible or rigid. Isolation of low-frequency vibration is studied, so that the passive mounts can be modelled as lumped parameter springs and dampers. Decentralized velocity feedback control is employed, where each actuator is operated independently by feeding back the absolute equipment velocity at the same location. Good control and robust stability have been obtained both theoretically and experimentally for the multichannel control systems. This is to be expected if the base structure is rigid, in which case the actuator and sensor are, in principle, collocated and the control system implements a skyhook damper. With a flexible base structure, however, collocation is lost due to the reactive actuator force acting on the base structure, but the control system is still found to be robustly stable and to perform well. Attenuations of 20 dB are obtained in the sum of squared velocities on the equipment structure at the rigid-body mounted resonance frequencies. In addition, attenuations of up to 15 dB are obtained at the resonance frequencies of both the low order flexible modes of the base structure and the equipment structure.

1. Introduction

Isolating a piece of delicate equipment from the vibration of a base structure is of practical importance in a number of engineering fields. Examples are the isolation of instrument boxes in aeroplanes and the isolation of telescopes and antennas in satellites. In the majority of cases, the

*Corresponding author. Current address: Mitsui Babcock Technology, Technology and Engineering Building, Porterfield Road, Renfrew PA4 8DJ, UK. Tel.: +44 141 8853509; fax: +44 141 8853668.

E-mail address: xhuang@mitsuibabcock.com (X. Huang).

0022-460X/03/$ - see front matter
doi:10.1016/S0022-460X(02)01057-X

base is flexible and vibrates with an unpredictable waveform which has a broadband spectrum. The active isolation of a vibration-sensitive equipment structure from a vibrating base is studied in this paper. Passive anti-vibration mounts are widely used to support the equipment and protect it from severe base vibration. However, conventional passive mounts suffer from an inherent trade-off between poor high-frequency isolation and amplification of vibration at the fundamental mounted resonance frequency [1]. Generally, the best isolation performance is achieved by using an active system in combination with a passive mount, where the fundamental resonance can be actively controlled without reducing the high-frequency performance.

When an active isolator is designed, two configurations are possible. The secondary actuator can be placed either in series or in parallel with the passive mount. Beard et al. [2] investigated the first configuration by coupling a piezoelectric actuator in series with a passive mount. However, the effectiveness of such a mounting design was shown to be heavily dependent upon the high stiffness of the actuators. Due to the small deflection capacity of piezoelectric actuators, the use of such actuation is limited to the isolation of very small amplitude motion of base structure. In many situations, the base vibration is of the order of millimetres. As a result, an actuator with a longer throw, such as electromagnetic shaker, is required. An experimental study was conducted by Serrand and Elliott [3] on the active vibration isolation of a rigid equipment structure using two electromagnetic shakers, which were installed in parallel with two passive mounts. An active isolator can be implemented using various feedback control strategies, among which independent velocity feedback control is one of the most popular. The absolute velocities of the equipment structure are measured at each mounting point and directly fed back to the actuators driving that point. Using independent velocity feedback control, Kim et al. [4] investigated a four-mount active vibration isolation system with a rigid equipment structure.

This paper investigates a similar four-mount system for active vibration isolation of a flexible equipment structure. Particular emphasis is placed on the isolation of low-frequency vibration (0–200 Hz), for which the mounts can be assumed to behave as lumped springs and dampers. The main objective is to investigate the control performance and stability issues associated with the four-mount vibration isolation system when the additional flexibility of the equipment structure is introduced. Active isolation experiments are first implemented on a rigid base before moving to the final flexible base, in order to have a full understanding of the control mechanisms. With the rigid base structure, the actuator force that reacts off the base has no effect on the equipment velocity and so the actuator force on the equipment and velocity sensor on the equipment are, in principle, collocated. It can be shown that under these conditions the control system is unconditionally stable. When the base structure is not rigid; however, the stability of the control system cannot be guaranteed a priori, because the equipment velocity is caused by both the actuator force acting directly on the equipment and the reactive actuator force causing the base to move, but a careful analysis has demonstrated that good stability properties are still obtained for the experiments described here. A theoretical model is derived for the dynamic response of the coupled system in Section 2. Section 3 is concerned with the stability of the controller and the practical implementation is described in Section 4. The performance of the control system with both the rigid and flexible base structure is discussed in Section 5 and in Section 6 the conclusions are summarized.

2. Theoretical analysis of the mounted active isolation structure

2.1. Single-mount active isolation system

Kim et al. [4] presented a simple model for the active vibration isolation of a single-mount system with a rigid equipment structure using the impedance method. This model is extended to study the active vibration isolation of a flexible equipment structure. Fig. 1(a) shows a one-dimensional mounted equipment structure, where the flexible equipment is supported by a passive mount consisting of a spring k_m and a damper c_m. The actuator, which generates a control force, f_c, is installed in parallel with the isolation system. In the practical implementation described below, the body of the actuator is mounted on the equipment structure and is arranged to drive through the passive mount. The mass of the actuator, m_a, thus has to be included in the model as shown in Fig. 1. The whole system on a general base structure can be represented in terms of mechanical impedance as shown in Fig. 1(b), where Z_a, Z_e, Z_m and Z_b denote the impedances of the actuator, flexible equipment, mount and the base structure, respectively. Compared to the electromagnetic shaker and the equipment, the mount is assumed to be massless in the frequency range of interest. For the convenience of the theoretical analysis, no time delay is assumed in the electric controller. The flexible base structure is excited by a primary force f_{pb}, and vibrates with a base velocity v_b, while f_{pe} denotes the excitation force acting on the equipment structure. Letting f_m denote the force acting through the mount on the equipment structure, the dynamics of the flexible equipment and the base structure are described by

$$(Z_e + Z_a)v_e = f_c + f_m + f_{pe}, \tag{1}$$

$$f_m = Z_m(v_b - v_e), \tag{2}$$

$$Z_b v_b = f_{pb} - f_m - f_c. \tag{3}$$

It is noted that in this one-dimensional analysis, the moment of inertia of the actuator cannot be taken into account. The impedances of the flexible equipment and the flexible base are obtained by inverting the corresponding mobilities Y_e and Y_b, while $Z_a = \mathrm{j}\omega m_a$ and $Z_m = (c_m + k_m/\mathrm{j}\omega)$, where $\mathrm{j} = \sqrt{-1}$. Combining Eqs (1)–(3), the dynamics of the system can be described in a

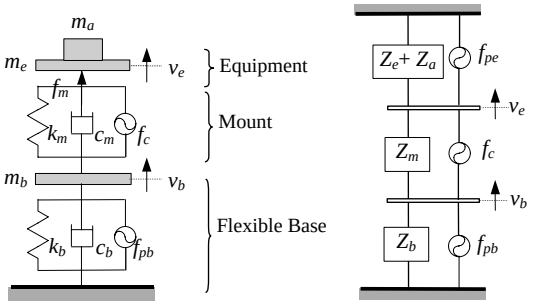

(a) Physical representation (b) Impedance representation

Fig. 1. Single-mount active vibration isolation system on a flexible base structure.

compact matrix form as follows:

$$\begin{bmatrix} Z_e + Z_a + Z_m & -Z_m \\ -Z_m & Z_b + Z_m \end{bmatrix} \begin{Bmatrix} v_e \\ v_b \end{Bmatrix} = \begin{Bmatrix} f_{pe} + f_c \\ f_{pb} - f_c \end{Bmatrix}. \tag{4}$$

Because the passive system is stable, the velocity responses can be obtained by inverting the impedance matrix in Eq. (4). In this paper, the control system employs the direct velocity feedback control strategy using the measured velocity signal v_e from the equipment structure to activate the actuator with a constant gain of $-h$. At low frequencies, the control force generated from the actuator is approximately proportional to the input velocity signal, i.e., $f_c = -hv_e$. Thus, Eq. (4) becomes

$$\begin{bmatrix} Z_e + Z_a + Z_m + h & -Z_m \\ -(Z_m + h) & Z_b + Z_m \end{bmatrix} \begin{Bmatrix} v_e \\ v_b \end{Bmatrix} = \begin{Bmatrix} f_{pe} \\ f_{pb} \end{Bmatrix}. \tag{5}$$

For a special case of a rigid base structure, $Z_b \to \infty$ and $v_b \to 0$, so that f_{pb} does not have any effect on the equipment structure. Therefore, the response of a flexible equipment structure on a rigid base to an excitation force acting on the equipment can be easily obtained from Eq. (5),

$$(Z_e + Z_a + Z_m + h)v_e = f_{pe}. \tag{6}$$

2.2. Multiple-mount active isolation system

The impedance representation of a single-mount flexible equipment structure can be generalized for the case where the flexible equipment structure is supported by a set of mounts as shown in Fig. 2. Without losing generality, the number of mounts under consideration is taken to be M, and the total number of modes in the flexible equipment structure is N. Since M mounts are used,

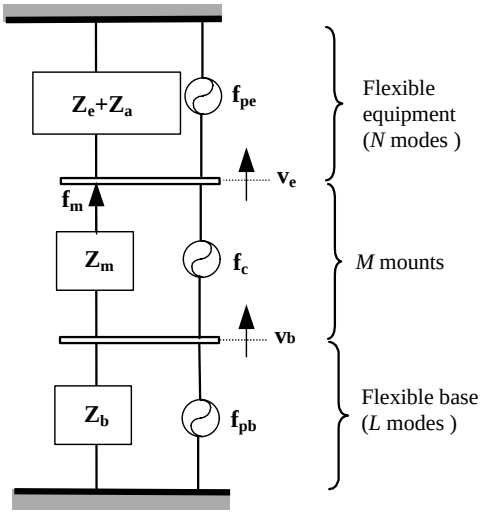

Fig. 2. Impedance representation of a multi-mount vibration isolation system.

the end velocities at the mount positions are denoted as M length vectors $\mathbf{v}_e$ and $\mathbf{v}_b$, at the flexible equipment and the flexible base structure respectively. Each mount has an actuator in parallel with it, providing an M length of secondary force vector $\mathbf{f}_c$. When the flexible base structure is excited at a number of arbitrary points by a primary force vector $\mathbf{f}_b$, the flexible base response can be described as

$$\mathbf{Z}_b\mathbf{v}_b = \mathbf{f}_{pb} - \mathbf{f}_m - \mathbf{f}_c, \tag{7}$$

where $\mathbf{f}_{pb} = \mathbf{Z}_b\mathbf{Y}_{bp}\mathbf{f}_b$ is the equivalent vector of primary forces at the mount positions giving that $\mathbf{Y}_{bp}$ is the mobility matrix of the uncoupled flexible base due to the vector $\mathbf{f}_b$ of forces acting on the base. By extending the Eqs. (1) and (2), combining with Eq. (7), the dynamic behaviour of the multi-mount active vibration isolation system with a flexible equipment structure on a flexible base can be described in matrix form as follows:

$$\begin{bmatrix} \mathbf{Z}_e + \mathbf{Z}_a + \mathbf{Z}_m & -\mathbf{Z}_m \\ -\mathbf{Z}_m & \mathbf{Z}_b + \mathbf{Z}_m \end{bmatrix} \begin{Bmatrix} \mathbf{v}_e \\ \mathbf{v}_b \end{Bmatrix} = \begin{Bmatrix} \mathbf{f}_{pe} + \mathbf{f}_c \\ \mathbf{f}_{pb} - \mathbf{f}_c \end{Bmatrix}. \tag{8}$$

The impedance matrices $\mathbf{Z}_a$ and $\mathbf{Z}_m$ are $(M \times M)$ diagonal matrixes, whose elements are the impedances due to the mass of each actuator, and the stiffness and damping of the corresponding mount, respectively. The impedance matrices $\mathbf{Z}_e$ and $\mathbf{Z}_b$ are determined from their corresponding mobility matrices $\mathbf{Y}_e$ and $\mathbf{Y}_b$.

Using decentralized velocity feedback control, each actuator is operated independently by feeding back the equipment absolute velocity with the same gain at each mount location. The control force vector $\mathbf{f}_c$ generated by the multiple actuators is then given by

$$\mathbf{f}_c = -\mathbf{H}\mathbf{v}_e, \tag{9}$$

where the control gain matrix $\mathbf{H}$ is diagonal. The system response of the multi-mount flexible equipment structure on a flexible base is obtained by substituting Eq. (9) into Eq. (8),

$$\begin{bmatrix} \mathbf{Z}_e + \mathbf{Z}_a + \mathbf{Z}_m + \mathbf{H} & -\mathbf{Z}_m \\ -(\mathbf{H} + \mathbf{Z}_m) & \mathbf{Z}_b + \mathbf{Z}_m \end{bmatrix} \begin{Bmatrix} \mathbf{v}_e \\ \mathbf{v}_b \end{Bmatrix} = \begin{Bmatrix} \mathbf{f}_{pe} \\ \mathbf{f}_{pb} \end{Bmatrix}. \tag{10}$$

In a similar manner to Eq. (6), the multi-mount flexible equipment structure on a rigid base can then be described by

$$(\mathbf{Z}_e + \mathbf{Z}_a + \mathbf{Z}_m + \mathbf{H})\mathbf{v}_e = \mathbf{f}_{pe}. \tag{11}$$

Conventionally, control performance is discussed in terms of transmissibility, which is defined by v_e/v_b for a single-mount active isolation system. However, the dynamic behaviour of the mounted flexible equipment structure is strongly coupled with the dynamics of the flexible base as can be seen from Eqs. (5) and (10). In this case, the velocity of the base structure changes with the control gain. Therefore, the transmissibility does not represent the absolute vibration response of the flexible equipment. It is thus preferable to use the absolute velocity of the flexible equipment structure as a control performance measure. The kinetic energy of the equipment structure has been suggested as a good measure of control performance when the equipment structure is rigid [4]. Considering the flexibility of the equipment studied, the true value of the kinetic energy will have components due to both the rigid-body modes and the flexible modes. An approximate estimate of the equipment kinetic energy can be obtained by taking the sum of squared values of

the equipment velocities at the mount locations, and this is used as a practical measure of control performance in this paper. This also means that the theoretical predictions can be easily compared with the experimental results.

3. Stability analysis

Let the matrix of frequency response functions between the actuator inputs, $\mathbf{f}_c$, and the sensor outputs, $\mathbf{v}_e$, be denoted $\mathbf{G}(\mathrm{j}\omega)$, which in control terms is known as the plant response matrix [5]. The block diagram of the feedback control system can then be drawn as in Fig. 3, where $\mathbf{d}$ is the vector of the sensor outputs due to the primary inputs acting alone, which acts as the disturbance on the system, and $\mathbf{H}(\mathrm{j}\omega)$ is the diagonal matrix of constant feedback gain h in this case, i.e.,

$$\mathbf{H}(\mathrm{j}\omega) = h\mathbf{I}, \tag{12}$$

where $\mathbf{I}$ is the identity matrix.

If the feedback control system is stable, the closed-loop output of the sensors is given by

$$\mathbf{v}_e = [\mathbf{I} + \mathbf{G}(\mathrm{j}\omega)\mathbf{H}(\mathrm{j}\omega)]^{-1}\mathbf{d}. \tag{13}$$

However, before this formula can be used to predict the performance of the control system, the stability of the multichannel feedback control system must be assured. This can be determined from the eigenvalues of the open-loop frequency response matrix, $\mathbf{L}(\mathrm{j}\omega) = \mathbf{G}(\mathrm{j}\omega)\mathbf{H}(\mathrm{j}\omega)$, using the generalised Nyquist criterion [5]. This states that, the control system is stable provided none of the loci of the eigenvalues encircles the $(-1, 0)$ point in the complex plane as ω varies from $-\infty$ to ∞.

In the case in which the base structure is rigid and decentralized feedback control is used, then

$$\mathbf{L}(\mathrm{j}\omega) = h\mathbf{G}(\mathrm{j}\omega), \tag{14}$$

where $\mathbf{G}(\mathrm{j}\omega)$ corresponds to the mobility matrix for a set of collocated force actuators and velocity sensors acting on the mounted equipment structure. The power supplied to this structure by the actuators is then equal to

$$\mathbf{\Pi} = \tfrac{1}{2}\,\mathrm{Re}[\mathbf{f}_c^{\mathrm{H}}\mathbf{v}_e] = \tfrac{1}{2}\,\mathrm{Re}[\mathbf{f}_c^{\mathrm{H}}\mathbf{G}(\mathrm{j}\omega)\mathbf{f}_c]. \tag{15}$$

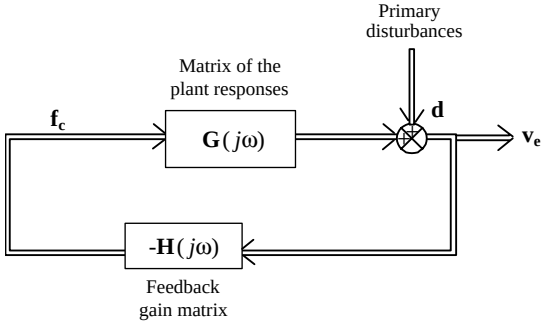

Fig. 3. Equivalent block diagram for a velocity feedback control system.

The plant response matrix is symmetrical in this case, due to reciprocity, and so the power supplied can also be written as

$$\mathbf{\Pi} = \tfrac{1}{2}\mathbf{f}_c^{\mathrm{H}}\,\mathrm{Re}[\mathbf{G}(\mathrm{j}\omega)]\mathbf{f}_c \tag{16}$$

which is only guaranteed positive if $\mathrm{Re}[\mathbf{G}(\mathrm{j}\omega)]$ is positive definite and so $\mathbf{G}(\mathrm{j}\omega)$ is passive. In this case the real parts of all the eigenvalues of $\mathbf{G}(\mathrm{j}\omega)$ must also be positive and so the locus of each of the eigenvalues of $\mathbf{L}(\mathrm{j}\omega)$ in this case are guaranteed to be on the right-hand side of the Nyquist plane. None of these loci can thus encircle the $(-1, 0)$ point and the system is unconditional stable.

This unconditional stability is not guaranteed when the base is flexible, however, because in this case $\mathbf{v}_e$ is not just as a result of the collocated actuator force at the top of the mount, but also has a component due to the reaction of the actuator force on the base structure. This reaction force causes base vibrations, which are transmitted to the equipment structure through the mounts. The plant response matrix thus does not correspond to the mobility matrix for a set of collocated forces and velocities, and its real part cannot be guaranteed to be positive definite.

4. Experimental investigation of the active vibration isolation

4.1. System description

A four-mount active vibration isolation system is built as illustrated in Fig. 4, and consists of a flexible equipment plate mounted on a base structure, which can either be rigid or flexible, through four anti-vibration mounts. The equipment structure consists of a 3.54 mm thick aluminium plate of dimensions $300 \times 160\,\mathrm{mm}^2$, which when loaded with the masses of the

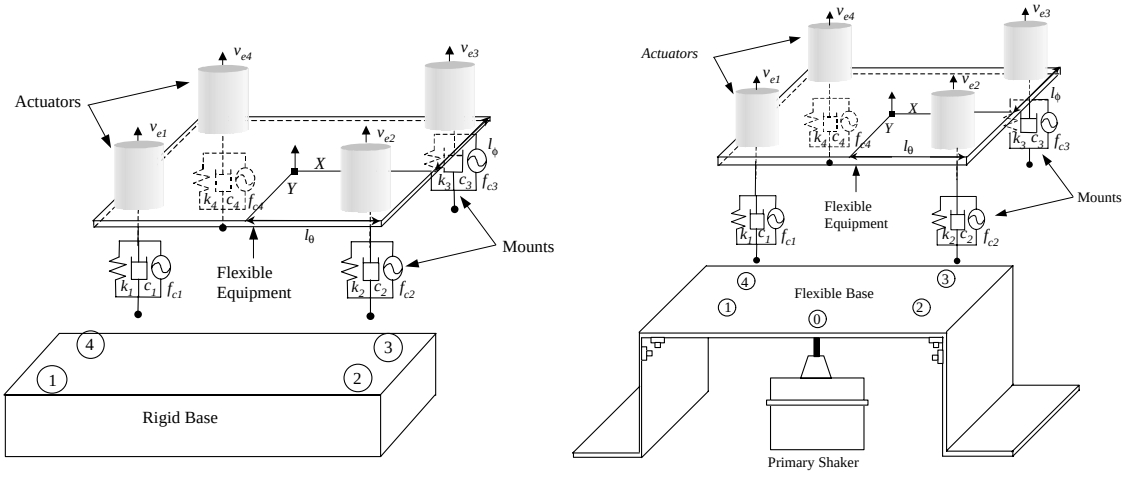

(a) Rigid base (b) Flexible base

Fig. 4. A four-mount active isolator for a flexible equipment structure.

actuators (0.91 kg each) is very flexible in the frequency range of interest. This flexible equipment structure together with the passive and active isolator is referred to as the mounted equipment structure in this paper. The passive mounts are made of natural rubber with a hollow cylindrical shape, and are bonded to the corners of the equipment plate via steel washers. Four electromagnetic shakers are rigidly installed on the top of the equipment plate at the corresponding mount positions by a set of bolts. A thin steel stinger inside each ring mount transmits the axial force generated by the control shakers to the supporting base via an aluminium disc, so that the control force can act in parallel with the passive isolator. The assembly at one corner of the mounted equipment structure is illustrated schematically in Fig. 5. The mounted equipment structure is first installed on a rigid base structure to identify its uncoupled dynamic characteristics before being moved to a flexible base. A thick steel plate with a large mass is used as the rigid base. For the flexible base, a thin steel rectangular plate of 2 mm thickness is used with its two long opposite edges bolted on to stiff frames, which has sufficient stiffness to support the mounted equipment structure. The other two edges of the flexible base structure remain free, which approximately realises a clamped–free–clamped–free boundary condition as defined by Warburton [6]. The control force generated from the shaker is proportional to the shaker current and thus to the shaker voltage, which is proportional to the input velocity signal. The calibration factors (force/voltage) for the shakers are determined, together with those of the sensors used (voltage/velocity) in order to be able to compare the absolute levels of the measurements taken from the experiments with the theoretical model. The physical and geometrical properties of the experimental set-up, as well as the locations of the mounts, are listed in Table 1.

In the experimental work, an FFT Analyzer (Advantest R9211C) is used to measure the velocity response of the equipment as well as generate the white-noise signal. When the mounted flexible equipment structure is excited, the acceleration signals at each mount location are measured using accelerometers (B&K type 4375). The acceleration signal is then passed to a general signal conditioner (B&K type 2635), which converts it to a velocity signal by an integrated module inside. Finally, each velocity signal is independently fed back to the corresponding actuator to implement decentralized feedback control. The velocity signals are also captured by the analyzer, so that the measured frequency responses can be compared with the predicted results to validate the theoretical model outlined in Section 2.

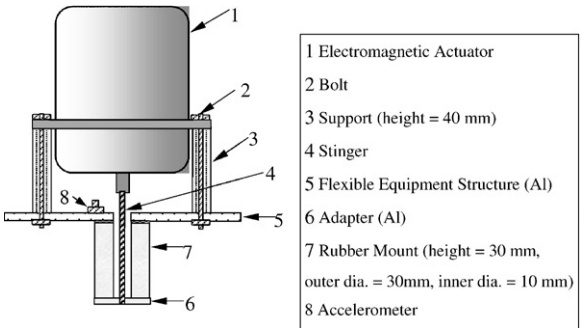

Fig. 5. Assembly at the corner of the mounted equipment structure.

Table 1
Physical properties and geometrical data of the active isolation system

Equipment structure	Material of the flexible equipment plate	Aluminium
	Density of the flexible equipment plate	2700 kg/m^3
	M_e, Mass of the flexible equipment plate	0.3564 kg
	Young's modulus	7.1×10^{10} N/m^2
	The Poisson ratio	0.33
	Damping ratio	$\zeta_e = 0.01$
	Dimensions of the flexible equipment plate (mm) ($L_{ex} \times L_{ey} \times t_e$)	$(160 \times 300 \times 3.54)$
Mount	k_m, Spring stiffness of each mount	1.2×10^4 N/m
	c_m, Damping of each mount	11.5 N s/m
	Mount locations on the flexible equipment (mm)	$l_\theta = 117$, $l_\phi = 47$
Base plate	Material	Steel
	Dimensions of the flexible base plate (mm) ($L_{bx} \times L_{by} \times t_b$)	$(500 \times 700 \times 2)$
	Damping ratio	$\zeta_b = 0.01$
Actuator	m_a, Mass of each actuator	0.91 kg
Location of mount 1 on the base plate (mm)		(250,350)
Location of mount 2 on the base plate (mm)		(250,584)
Location of mount 3 on the base plate (mm)		(156,584)
Location of mount 4 on the base plate (mm)		(156,350)
Location of the primary force on the base plate (mm)		(320,270)

4.2. Model validation

The active vibration isolation system used in the experiment was simulated using the theoretical model outlined in Section 2. The stiffness and damping properties of the passive mounts were chosen in order to best fit the measured fundamental natural frequency and bandwidth. In order to match the frequency of the measured first flexible resonance of the plant response, the thickness of the flexible equipment plate in the theoretical model was set to be 2.9 mm instead of 3.54 mm.This lowers the frequency of the first flexible mode of the active isolator and is thought to compensate for the frequency lowering effect of the rotational moments of inertia of the shakers in the experimental arrangement, which were not accounted for in the theoretical model.

The theoretical plant responses are calculated when the mounted equipment structure is installed on both a rigid and a flexible base structure. For validation purposes, the experimental (solid line) and simulation (dashed line) results are shown together in Fig. 6 for the plant response G_{11} at mount 1, which is the (1,1) element of the plant matrix $\mathbf{G}(j\omega)$. The theoretical result matches reasonably well with the experimental one for a rigid base case as shown in Table 2. The experimental results below 5 Hz have low coherence due to the low sensitivity of the actuator and sensor used, and result in some discrepancies from the predictions. On a rigid base as shown in Fig. 6(a), the predicted resonance frequencies of the three rigid-body modes (heave motion at 17.40 Hz, pitch motion at 17.78 Hz and roll motion at 17.43 Hz) are so close that they merge into one large peak, which is in accordance with the measured results from the experiment. The frequency of the first flexible mode of the mounted flexible equipment structure is predicted to be

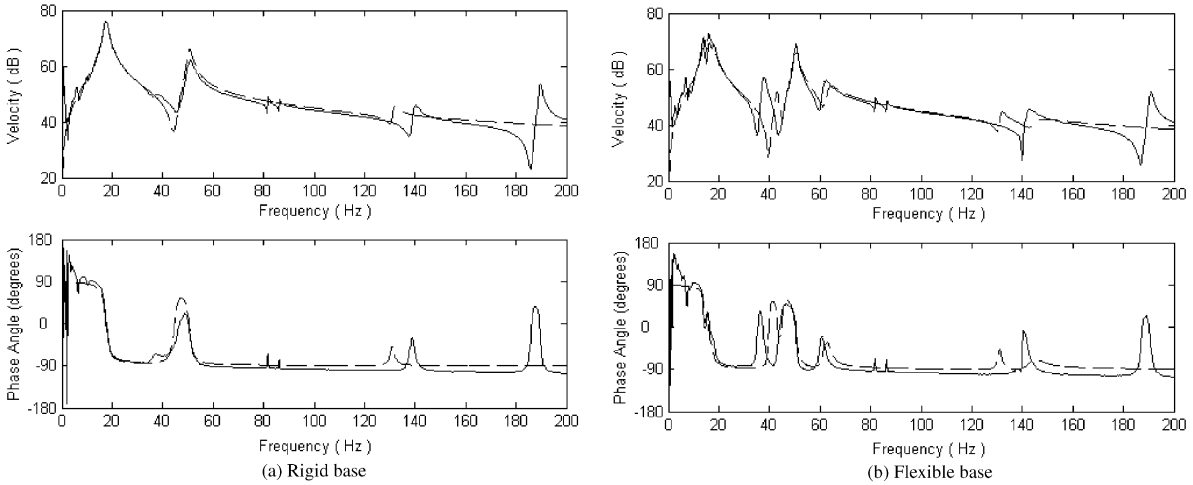

Fig. 6. Plant responses at mount 1 when only the actuator at mount 1 is active.

Table 2
Natural frequencies of the mounted flexible equipment structure on a rigid base

Simulation						Experiment					
Frequency (Hz)	Motion	Mode shape				Frequency (Hz)	Motion	Mode shape			
		1	2	3	4			1	2	3	4
17.40	Heave	+	+	+	+	17.42	Heave	+	+	+	+
17.78	Pitch	+	—	—	+	17.98	Pitch	+	—	—	+
17.42	Roll	+	+	—	—	17.45	Roll	+	+	—	—
50.6	Flexible (Torsion)	+	—	+	—	50.5	Flexible (Torsion)	+	—	+	—
132.1	Flexible (Heave)	+	+	+	+	140.0	Flexible (Pitch)	+	—	—	+
						189.6	Flexible (Torsion)	+	—	+	—

about 50.5 Hz, with the second at about 132.1 Hz. In the experimental results, the second resonance occurs at about 140 Hz and a third flexible mode of the equipment structure is observed at about 190 Hz which is not predicted by the simulation in the frequency range.

The theoretical and experimental plant responses of G_{11} at mount 1 with the equipment structure installed on the flexible base are also compared in Fig. 6(b) with the individual resonance frequencies listed in Table 3. The plant response is now a coupled response between the mounted equipment and the base structures. The first three dominant peaks from the experiment correspond to the rigid-body modes of the mounted equipment structure (heave motion at 14.0 Hz, pitch motion at 16.8 Hz, and roll motion at 18.0 Hz), which are again reasonably close to those predicted from the simulation (14.3, 16.0 and 17.2 Hz). The peaks due to the flexible equipment structure resonances are similar to those for the rigid base structure case. Other peaks

Table 3
Natural frequencies of the mounted flexible equipment structure on a flexible base

Simulation						Experiment					
Frequency (Hz)	Motion	Mode shape				Frequency (Hz)	Motion	Mode shape			
		1	2	3	4			1	2	3	4
14.3	Heave	+	+	+	+	14.0	Heave	+	+	+	+
16.0	Pitch	+	—	—	+	16.3	Pitch	+	—	—	+
17.2	Roll	+	+	—	—	18.0	Roll	+	+	—	—
50.5	Flexible (Torsion)	+	—	+	—	50.5	Flexible (Torsion)	+	—	+	—
131.7	Flexible (Heave)	+	+	+	+	142.1	Flexible (Pitch)	+	—	—	+
						190.7	Flexible (Torsion)	+	—	+	—

show the influence of the flexible base structure, which can be distinguished by comparison with Fig. 6(a). These occur at about 40 and 62 Hz, for example. Some discrepancies between the experiments and simulations over 30 Hz are due to the imperfect physical realisation of the clamped–clamped boundary condition. The simulations are otherwise found to be in reasonable agreement with the experimental results for all 16 elements of the plant response matrix $\mathbf{G}(j\omega)$. The dynamics of the four-mount flexible equipment structure can be thus investigated to within a satisfactory accuracy using the theoretical model.

4.3. Stability assessment

For the four-mount equipment structure, the (4×4) plant response matrix $\mathbf{G}(j\omega)$ has four frequency-dependent eigenvalues. In order to be able to represent these eigenvalues as smooth functions of frequency; however, some care needs to be taken in their calculation, as discussed in the appendix. Fig. 7 shows the eigenvalue loci from both the simulated and measured responses for the rigid base case, while Fig. 8 shows those for the flexible base case. Apart from some differences in resonant amplitudes, the theoretical results match fairly well with those from the experiment except at frequencies below 5 Hz.This further validates the theoretical model developed for the four-mount flexible equipment structure. It is clear that none of the eigenvalue loci from the simulations cross the negative real axis, which indicates that the flexibility of the equipment structure does not cause instability. This is to be expected for the rigid base case, as discusses in Section 3, but is an important observation for the flexible base case. In practice, the eigenvalue loci from the experimental data slightly cross the negative real axis in both cases because of the phase shifts in the electronics of the control loop at very low frequencies. In addition, relatively small loops are observed to cross the negative real axis in the middle of the frequency band of analysis in Fig. 7. This is thought to result from the fact that the sensor and actuator are not exactly collocated in the experiment, as shown in Fig. 5, and because of the flexibility of the equipment structure. These loops cannot encircle the $(-1, 0)$ point, however, and therefore do not threaten the stability of the control system. Therefore, good control stability is

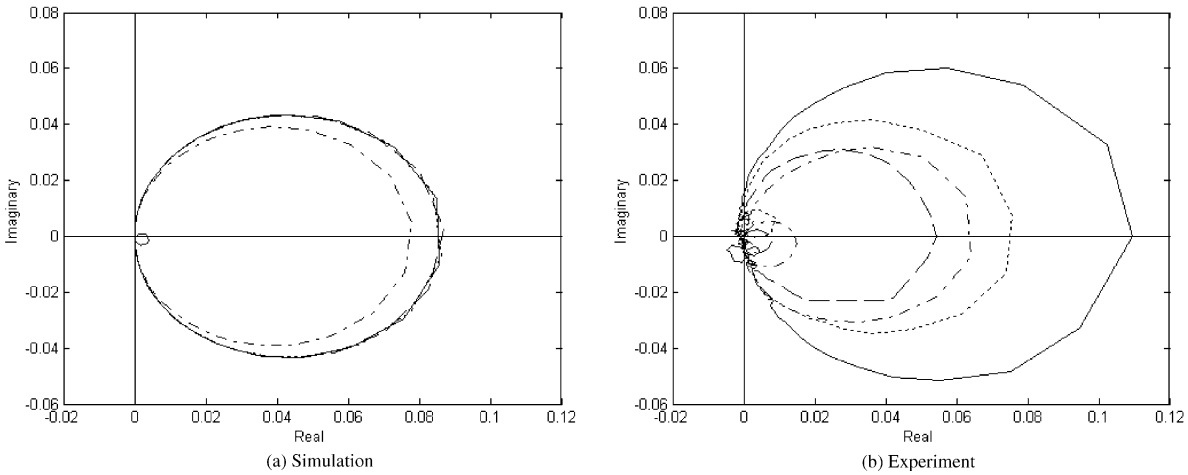

Fig. 7. Eigenvalue loci of the plant responses of the four-mounted active vibration.

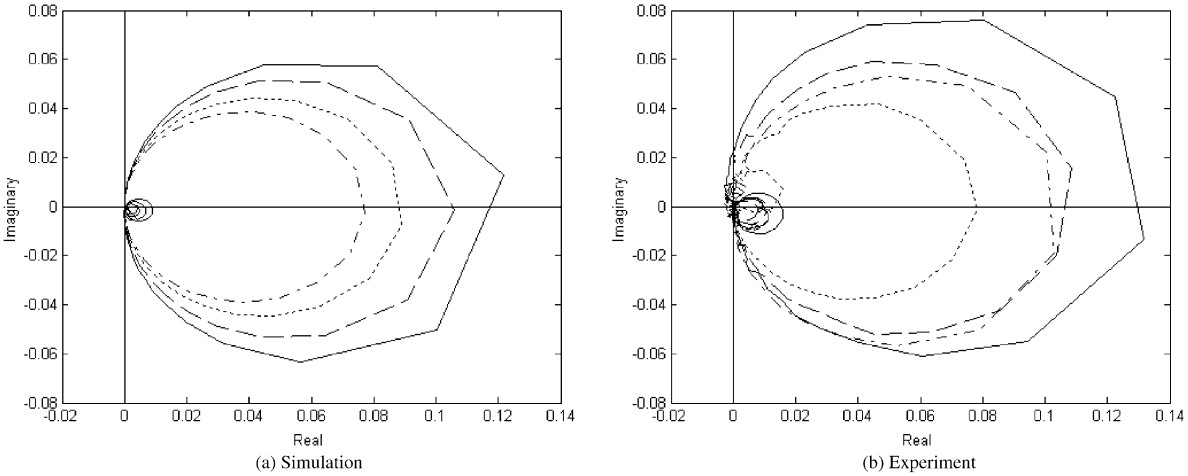

Fig. 8. Eigenvalue loci of the plant responses of the four-mounted active vibration.

expected for decentralized velocity feedback control in practice. The main threat to the control stability arises from the phase shifts in the electronics of the control loop at low frequencies. The comparison between the simulation and measured eigenvalue loci for the equipment on the flexible base is also good as seen from Fig. 8. The smaller loops are now due to the flexible modes of both the equipment structure and the base structure, but both occur on the right hand side of the Nyquist plot.

5. Control performance

A single-channel velocity feedback control system is implemented on each of the four mounts when the flexible equipment structure is mounted on either a rigid or the flexible

base structure in the experiments. Each feedback channel has an equal, constant, feedback control gain. The feedback control gain used here refers to the gain relating the secondary actuator force to the control velocity in units of N s/m. This convention is adopted so that the feedback control gain used in the experiments can be directly compared with that used in the simulations and must account for the different gains used in the feedback loop in the experiments, which comprises the charge amplifier gain K_{ca}, the power amplifier gain K_{pa}, and the sensitivity of the actuator K_a (equal to 0.91 N/V). The sensitivity of the accelerometer and the time constant of the integrator are directly taken into account by the charge amplifier when it is set properly, so that $K_{ca} = 100$ V/ms. Therefore, the feedback control gain, in units of N s/m, is calculated as

$$h = K_a K_{pa} K_{ca}. \tag{17}$$

The control performance of the multichannel velocity feedback system was investigated with the flexible equipment structure on both a rigid and a flexible base structure using different feedback gains. As an example, a feedback gain of 364 N s/m corresponds to a control gain of 40 from the power amplifier.

5.1. Control performance on a rigid base structure

Fig. 9 shows the predicted values of the absolute velocities of the flexible equipment at the four-mount locations for three different feedback gains when the mounted equipment structure is installed on a rigid base structure, while the corresponding results from the experiments are shown in Fig. 10. The responses before control are shown in thick lines and the responses after control in thin lines. The three thin solid curves correspond to a series of feedback gains of 182, 910 and 2002 N s/m, which are calculated from Eq. (17) for power amplifier gains of 2, 10 and 22, respectively. The control performances from the simulation agree reasonably well with the experimental results except at very low frequency due to the phase shifts in the electronic equipment used in the experiment. Reductions of up to 30 dB are observed in vibration level at the resonance frequencies of the rigid-body modes, and up to 20 dB reduction is observed at the first equipment structure resonance frequency of 50.5 Hz. Reductions in vibration level of nearly 10 dB at the second and the third flexible resonance frequencies of the mounted equipment structure are also obtained in the experiment, even though the simulations only predict 3–4 dB attenuation. The rigid-body resonances as well as the first flexible resonance are no longer noticeable after control with the highest value of feedback gain. Some amplification of the very low-frequency response of the flexible equipment structure can be observed in the experiments due to the effect of instrumentation phase shifts. Good stability of the four-channel control system on a rigid base is found as a maximum feedback control gain of 10 920 N s/m could be applied before the control system goes unstable. The gain margin of the four-channel velocity feedback control system is thus about 14 dB even for the highest gain in Fig. 10.

The overall control performance is further assessed using an estimate of the kinetic energy of the equipment structure represented by the sum of the squared velocity signals at all four mount positions. A comparison between the predicted and the experimental results is shown in Fig. 11. It is evident that the multichannel decentralized velocity feedback control is

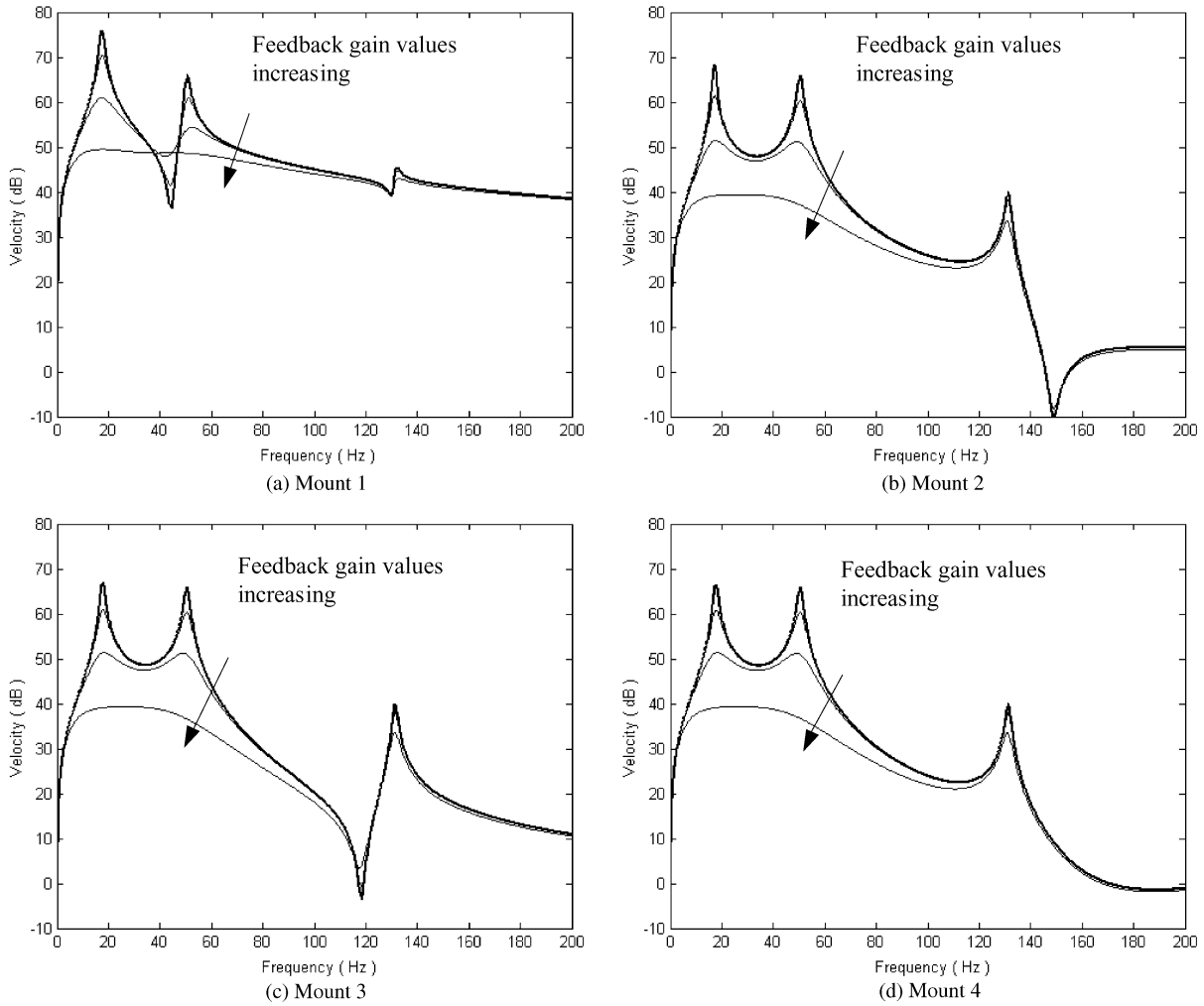

Fig. 9. Simulation results of the equipment velocity responses on a rigid base.

effective in attenuating the vibration levels at all resonance frequencies of interest. In particular, both theory and experiment give a reduction of up to 30 dB in the sum of squared velocities at the resonance frequencies of the rigid-body modes of the mounted equipment structure, and up to 20 dB at the first flexible frequency of 50.5 Hz. As the passive isolation performance increases, the control effect decreases and only 1–2 dB reductions are obtained at 200 Hz.

5.2. *Control performance on a flexible base structure*

The multichannel decentralized velocity feedback control is also implemented experimentally when the mounted equipment structure is installed on a flexible base structure. Similar feedback

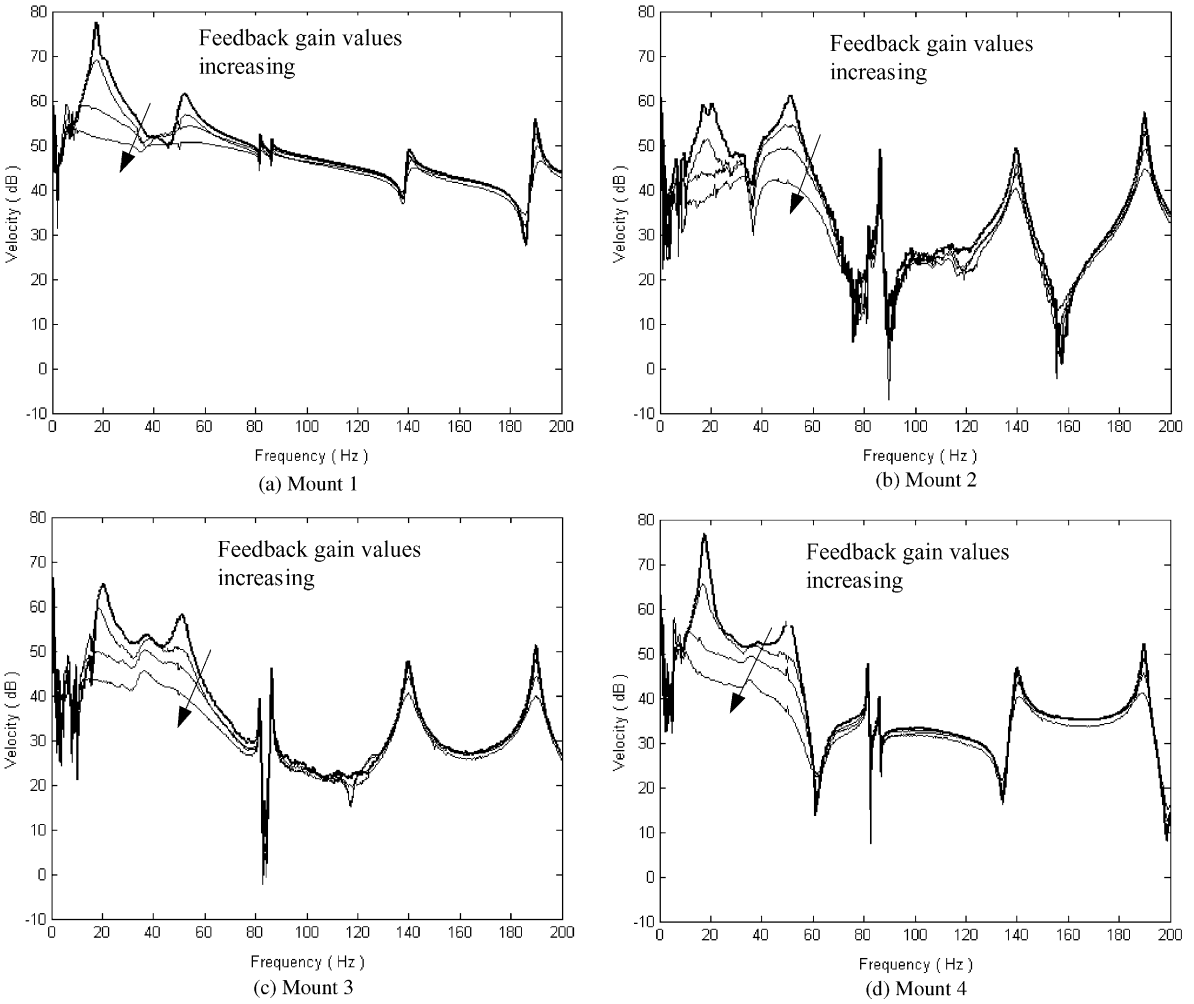

Fig. 10. Experimental results of the equipment velocity responses on a rigid base.

gains as used in the case of a rigid base are applied in the multichannel control experiments on a flexible base structure. The predicted velocity responses of the equipment structure before control (thick lines) and after control (thin lines) at all four mount locations are shown in Fig. 12, while the experimental results are illustrated in Fig. 13. Compared with Figs. 9 and 10 for the rigid base case, it can be seen that the dynamics of the flexible base is now strongly coupled with that of the equipment structure, and has a strong influence on the equipment velocity responses. The vibration levels at the resonance frequencies of the mounted equipment structure are greatly attenuated at all four mount positions. In particular, reductions in vibration level of up to 25 dB at the rigid-body modes at around 17 Hz, up to 20 dB at 50.5 Hz, can be achieved with the highest value of feedback gain in practice. For the vibrations at the base resonance frequencies, however, different levels of attenuation are observed. At mounts 1 and 4, the vibration levels at all the base plate resonance frequencies are effectively reduced both theoretically and experimentally.

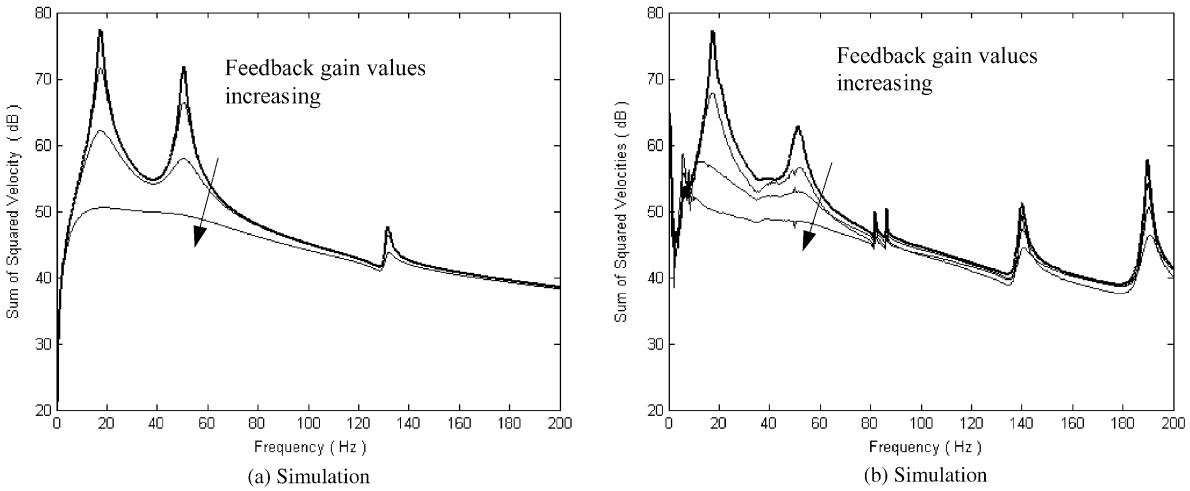

Fig. 11. Sum of square values of velocities of the flexible equipment on a rigid base.

However, the vibrations at several base resonance frequencies are slightly amplified in practice as seen from Fig. 13(c) at about 33 Hz at mount 3. The experimental response is similar to that predicted at the corresponding base resonance frequency of about 43 Hz at mount 3 as seen in Fig. 12(c). The velocity response at other positions, for example at the centre of the equipment plate, can also be obtained from the simulation and an examination of these shows that a global reduction in vibration level of the mounted equipment structure has been obtained.

The overall control performance of the active vibration isolation system is investigated using the sum of the square values of the equipment velocities at each corner position as shown in Fig. 14. The results before control are illustrated in thick lines and those after control in thin lines both theoretically and experimentally with three different feedback gains. The predictions agreed reasonably well with the experimental results, and clearly demonstrated that the vibration levels could be effectively attenuated over the frequency band of interest. In particular, up to 25 dB reductions in the sum of squared velocities at the rigid-body modes of the mounted equipment structure, as well as up to 20 dB reduction at the resonances caused by the low order flexible modes of the coupled base and equipment structure, can be achieved in practice. If the sum values of squared velocities at a large number of points on the equipment plate are calculated, very similar results to those shown in Fig. 14 are obtained. Thus the flexibility of the supporting base structure has not significantly affected the control stability and it is found that the gain margin is approximately the same as in the case of a rigid base structure.

6. Conclusions

Active vibration isolation has been investigated both theoretically and experimentally for a four-mount equipment structure, in which electromagnetic actuators are installed in parallel with each of four mounts placed between a flexible equipment and a supporting base structure.

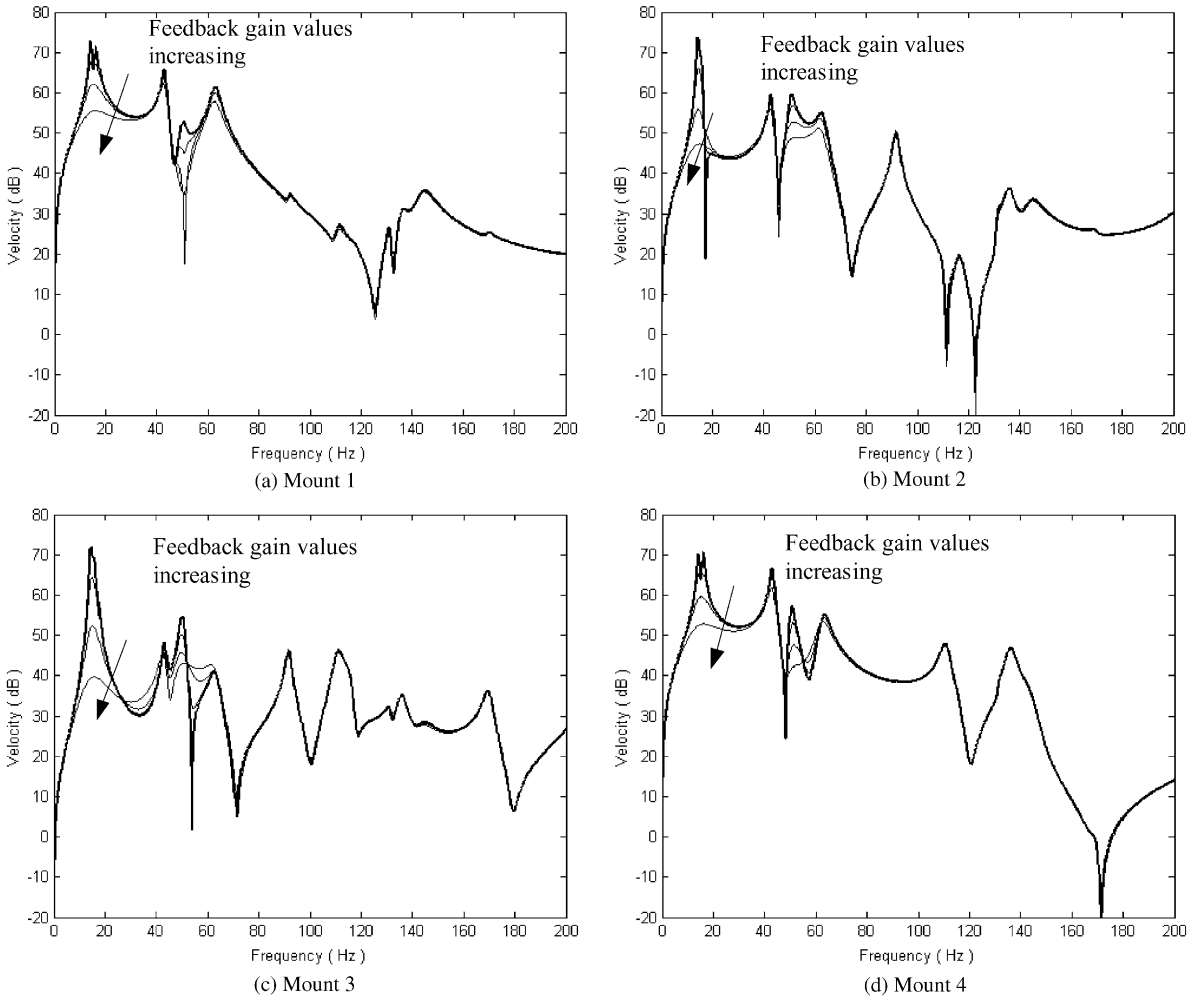

Fig. 12. Simulation results of the equipment velocity responses on a flexible base.

Decentralized velocity feedback control is implemented experimentally to actively isolate the vibration at frequencies up to 200 Hz. With a rigid base, unconditional stability of the multichannel control system is theoretically guaranteed regardless of the flexibility of the equipment structure. In practice, good control performance is observed with a gain margin of about 14 dB. The phase shifts in the electronics of the control loop at low frequencies and the non-collocated installation of the sensor and actuator due to the flexibility of the equipment and base structures are found to be the main threats to the control stability in practice. It is also found that this robust stability is carried over to the case when the base structure is a flexible plate. Control performance, in terms of squared velocities of the equipment structure, demonstrates that the multichannel active isolation system can effectively reduce the vibration of the equipment structure over a wide frequency range.

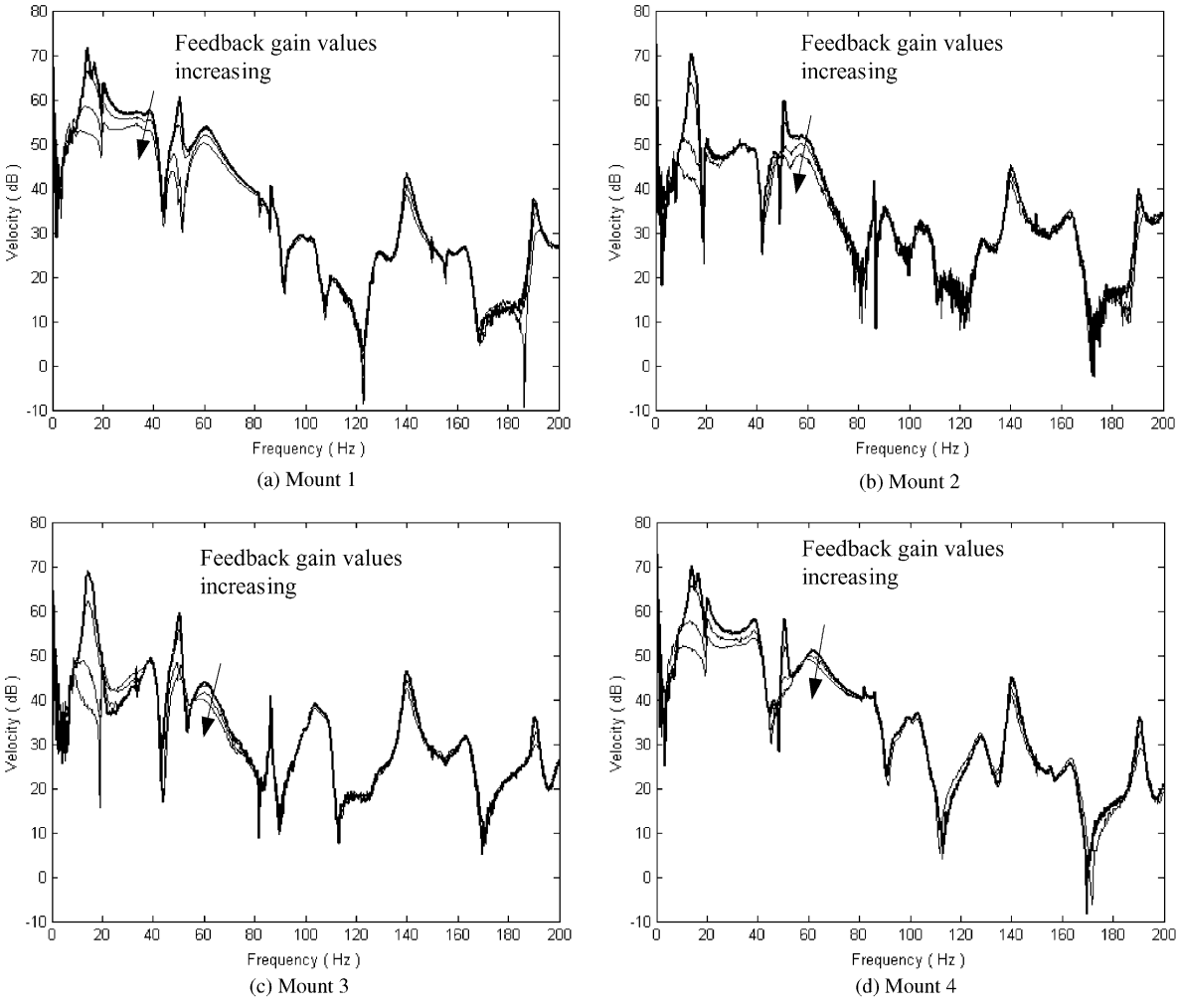

Fig. 13. Experimental results of the equipment velocity responses on a flexible base.

Appendix A. An algorithm to obtain the eigenvalues in order

There is an inherent numerical difficulty in obtaining a smooth plot of the frequency response for the eigenvalues of a plant response matrix within MATLAB, because the built-in functions automatically sort the calculated eigenvalues in a predefined order. For example, the eigenvalues of a real symmetric matrix are sorted in an ascending order. A typical plot of the eigenvalues of the experimental plant response matrix directly obtained from MATLAB is shown in Fig. 15. The first eigenvalue is always assigned to be λ_1, the next is assigned to be λ_2, etc. As the individual eigenvalues cross over, there is thus a physically unrealistic discontinuity in their slope. This makes it very difficult to evaluate the stability of the multichannel control system. An algorithm has therefore been developed to distinguish each of the smoothly varying eigenvalues from one another, using the corresponding eigenvectors.

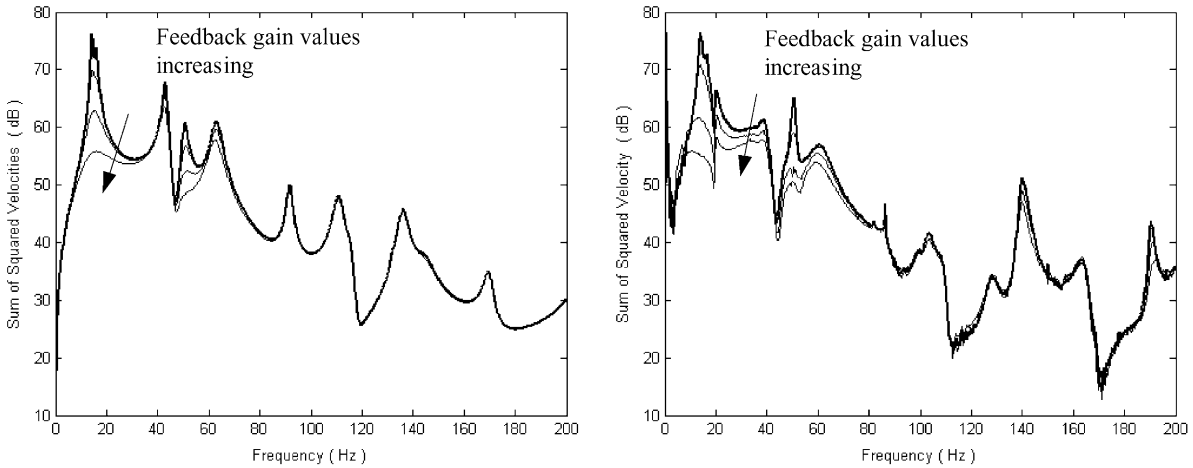

Fig. 14. Sum of squared values of velocities of the flexible equipment on a flexible base.

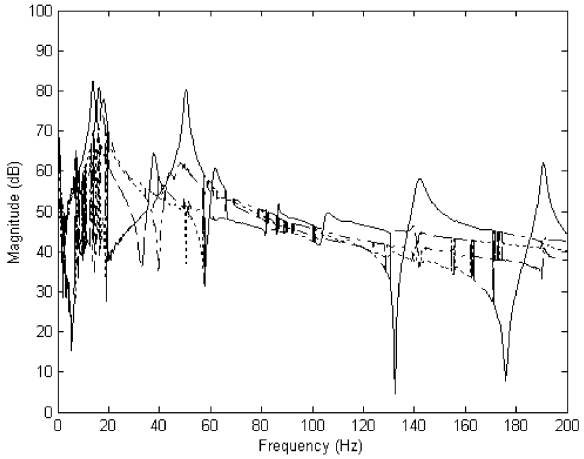

Fig. 15. Magnitudes of the eigenvalues before data treatment.

The relationship between the plant response matrix $\mathbf{G}(j\omega)$ and its eigenvalue matrix $\Omega(j\omega)$ can be expressed by

$$\mathbf{G}(j\omega)\mathbf{Q}(j\omega) = \mathbf{Q}(j\omega)\mathbf{\Omega}(j\omega), \tag{A.1}$$

where $\mathbf{\Omega}(j\omega)$ is a diagonal matrix of the eigenvalues $\lambda_i(j\omega)$, and $\mathbf{Q}(j\omega)$ is the matrix of the corresponding eigenvectors of the plant response matrix $\mathbf{G}(j\omega)$ at the frequency ω. At a frequency ω_1, the eigenvectors may be denoted as $\mathbf{q}_1(j\omega_1), \mathbf{q}_2(j\omega_1), \ldots, \mathbf{q}_n(j\omega_1)$ (in this paper, $n = 4$), and have the property that $\mathbf{q}_i^{\mathrm{H}}(j\omega_1)\mathbf{q}_i(j\omega_1)$ is of order 1. Similarly, the eigenvectors at an adjacent frequency ω_2 maybe be denoted as $\mathbf{q}_1(j\omega_2), \mathbf{q}_2(j\omega_2), \ldots, \mathbf{q}_n(j\omega_2)$, etc., although the ordering of the eigenvalues

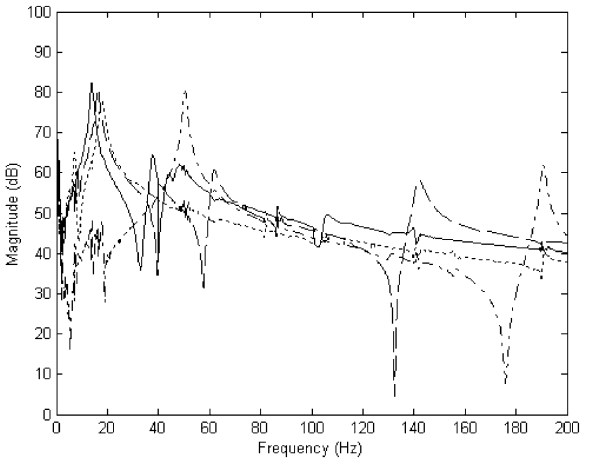

Fig. 16. Magnitude of the eigenvalues after data treatment.

and hence of the eigenvectors may has changed. The inner product of each eigenvector at frequency ω_1 with each eigenvector at frequency ω_2 is then calculated as

$$\mathbf{q}_l^{\mathrm{H}}(\mathrm{j}\omega_1)\mathbf{q}_m(\mathrm{j}\omega_2) = a_{lm}. \tag{A.2}$$

If the two eigenvectors are similar, the magnitude of a_{lm} will be of order 1 and if they are dissimilar, the magnitude of a_{lm} will be of order 0. In this way, similar eigenvectors and hence their associated eigenvalues can be traced from one frequency to another. Fig. 16 shows the eigenvalues calculated using this algorithm for the same experimental plant response matrix as was used to generate Fig. 15, which are now smoothly varying functions of frequency and so can be used to plot meaningful Nyquist plots in order to assess stability.

References

[1] C.E. Crede, J.E. Ruzicka, Shock and Vibration Handbook, McGraw-Hill, New York, 1996.
[2] M.J. Beard, A.H. Von Flotow, D.W. Schubert, A practical product implementation of an active/passive vibration isolation system, Proceedings of IUTAM Symposium on the Active Control of Vibration, University of Bath, UK, 1994, pp. 101–108.
[3] M. Serrand, S.J. Elliott, Multichannel feedback control for the isolation of base-excited vibration, Journal of Sound and Vibration 234 (4) (2000) 681–704.
[4] S.M. Kim, S.J. Elliott, M.J. Brennan, Decentralised control for multichannel active vibration isolation, IEEE Transactions on Control Systems Technology 9 (1) (2001) 93–100.
[5] S. Skogestad, I. Postlethwaite, Multivariable Feedback Control; Analysis and Design, Wiley, New York, 1996.
[6] G.B. Warburton, The vibration of rectangular plates, Proceedings of the Institution of Mechanical Engineering 168 (1951) 371–384.